Simulation study of a magnetocardiogram based on a virtual heart model: effect of a cardiac equivalent source and a volume conductor*

Shou Guo-Fa(寿国法)[a)], Xia Ling(夏 灵)[a)†], Ma Ping(马 平)[b)], Tang Fa-Kuan(唐发宽)[c)‡], and Dai Ling(戴 灵)[a)]

[a)] *Department of Biomedical Engineering, Key Laboratory for Biomedical Engineering of the Ministry of Education, Zhejiang University, Hangzhou* 310027, *China*

[b)] *Department of Physics, State Key Laboratory for Artificial Microstructure and Mesoscopic Physics, Peking University, Beijing* 100871, *China*

[c)] *Department of Cardiology, the 309th Hospital of the People's Liberation Army, Beijing* 100091, *China*

(Received 5 August 2010; revised manuscript received 8 September 2010)

In this paper, we present a magnetocardiogram (MCG) simulation study using the boundary element method (BEM) and based on the virtual heart model and the realistic human volume conductor model. The different contributions of cardiac equivalent source models and volume conductor models to the MCG are deeply and comprehensively investigated. The single dipole source model, the multiple dipoles source model and the equivalent double layer (EDL) source model are analysed and compared with the cardiac equivalent source models. Meanwhile, the effect of the volume conductor model on the MCG combined with these cardiac equivalent sources is investigated. The simulation results demonstrate that the cardiac electrophysiological information will be partly missed when only the single dipole source is taken, while the EDL source is a good option for MCG simulation and the effect of the volume conductor is smallest for the EDL source. Therefore, the EDL source is suitable for the study of MCG forward and inverse problems, and more attention should be paid to it in future MCG studies.

Keywords: virtual heart model, magnetocardiogram, dipole source, equivalent double layer source, volume conductor model

PACS: 07.05.Tp **DOI:** 10.1088/1674-1056/20/3/030702

1. Introduction

The magnetocardiogram (MCG) is a noninvasive and noncontact technique for measuring the weak magnetic signals generated by cardiac electrophysiological activities. MCG and electrocardiography (ECG) have essentially the same cardiac ionic current signal generator, however, they have different performances and sensitivities to the cardiac activity due to the different characteristics of the electric and magnetic fields, and the complicated relationship between the MCG and the ECG has not been fully clarified.[1] Although the MCG has not yet been accepted as a routine clinical tool in hospitals like the standard 12-lead ECG has, it has proved to be superior to the ECG for the diagnosis of several cardiac diseases like myocardial ischemia, arrhythmias, fetal heart, *etc.* and in cardiac source location, etc.[2−8] Unfortunately, there are still many debates about the widespread clinical application of MCG diagnosis due to the lack of clinical equipment and evidence-based information about the clinical benefits.

In addition to the experimental studies of MCGs,[2,3,7,9] including the advancement of superconducting quantum interface device (SQUID),[10−13] cardiac computer modeling, developed as a useful tool to investigate the cardiac physiology and pathology, has been used in MCGs. MCG research, combined with a cardiac model, includes the forward problem of the generation analysis of MCG and MCG patterns according to various cardiac activities,[3,14−18] and the inverse problem of the MCG mapping of cardiac information.[7,18−22] The former is to calculate the cardiac electromagnetic field on the torso surface,

*Project supported by the State Key Development Program for Basic Research of China (Grant Nos. 2007CB512100 and 2006CB601007), the National Natural Science Foundation of China (Grant No. 10674006), the National High Technology Research and Development Program of China (Grant No. 2007AA03Z238), China Postdoctoral Science Foundation (Grant No. 20090461376), and the Fundamental Research Funds for the Central Universities (Grant No. KYJD09001).

†E-mail: xialing@zju.edu.cn

‡E-mail: tfk616@yahoo.com.cn

© 2011 Chinese Physical Society and IOP Publishing Ltd

while the latter is to reconstruct/recover the cardiac electrophysiological information from the measured ECG/MCG.

In the cardiac problem, cardiac equivalent source models are often used to theoretically represent the cardiac activities and applied to forward and inverse calculations of ECG/MCG. The commonly used cardiac equivalent sources are current dipole source, current multipole source and equivalent double layer (EDL) source.[23] For the MCG problem, the former two are often used,[7,17−22,24] while the latter one is seldom taken.[25] The different performances of the MCG generated from these source models have not been presented before. Meanwhile, it has been found that the torso volume conductor model has little effect on the MCG[17,19] and is always neglected in the MCG inverse problem due to the difficulty of its construction. However, the different influences of the volume conductor combined with the different source models on the MCG have seldom been studied.

In the present paper, we carry out the MCG simulation study using the boundary element method (BEM), based on the virtual heart electrophysiological model and the realistic torso volume conductor model. First, we describe and compare the dipole source model and the EDL source model in terms of the simulated MCG. For the dipole source, we used 1 dipole and 53 dipoles to macroscopically represent the heart separately. The results from the 53 dipoles serve as the reference to investigate other solutions. Then, combined with these cardiac source models, the contribution of the volume conductor model to the MCG is analysed. Finally, some conclusions are summarized about the source models and the volume conductor.

2. Theory and method

In the quasi-static approximation, the electric potential Φ can be expressed by Poisson equation as

$$\begin{cases} \nabla\cdot(\sigma\nabla\Phi) = \nabla\cdot\boldsymbol{J}_{\rm P}, \text{ in } \ \Omega, \\ \sigma(\nabla\Phi)\cdot\boldsymbol{n} = 0, \qquad \text{on } \ S_{\rm B}, \end{cases} \tag{1}$$

where σ is the electric conductivity, $\boldsymbol{J}_{\rm P}$ is the primary current density, $\boldsymbol{n}$ is the outward normal vector, Ω is the volume conductor and $S_{\rm B}$ is the body surface. The magnetic field $\boldsymbol{B}(\boldsymbol{r})$ due to the total current density $\boldsymbol{J}$ is obtained based on the Biot–Savart law as

$$\boldsymbol{B}(\boldsymbol{r}) = \frac{\mu_0}{4\pi}\int_{V'}\frac{\boldsymbol{J}(\boldsymbol{r}')\times\boldsymbol{R}}{R^3}{\rm d}v', \tag{2}$$

where V' is the volume containing all active sources, and μ_0 is the magnetic permeability of the vacuum, $\boldsymbol{R}$ is $\boldsymbol{r}-\boldsymbol{r}'$, with $\boldsymbol{r}$ being the field point and $\boldsymbol{r}'$ the source point. In the cardiac electromagnetic field, the total current density $\boldsymbol{J}$ contains the primary current density $\boldsymbol{J}_{\rm P}$ and the ohmic volume current density $\boldsymbol{J}_{\rm V}$. The $\boldsymbol{J}_{\rm V}$ is induced by $\boldsymbol{J}_{\rm P}$ due to the changed conductivities of different organs. It exists on the interfaces of different organs, and can be written as

$$\boldsymbol{J}_{\rm V} = -\sigma\nabla\Phi. \tag{3}$$

Solving Eqs. (1) and (2) using the BEM method, the integral equations for the cardiac electric and the magnetic field can be obtained as[16,26]

$$\begin{aligned} \Phi(\boldsymbol{r}) &= \frac{\sigma_{\rm s}}{\bar{\sigma}}\Phi_\infty(\boldsymbol{r}) \\ &\quad + \frac{1}{4\pi\bar{\sigma}}\sum_{l=1}^{m}(\sigma_l^- - \sigma_l^+)\int_{S_l}\Phi(\boldsymbol{r}')\nabla\frac{1}{\boldsymbol{R}}\cdot\boldsymbol{n}{\rm d}s', \\ \Phi_\infty(\boldsymbol{r}) &= -\frac{1}{4\pi\sigma_{\rm s}}\int_{V_{\rm H}}\boldsymbol{J}_{\rm P}(\boldsymbol{r}')\cdot\nabla\frac{1}{\boldsymbol{R}}{\rm d}V'_{\rm H}, \qquad (4) \\ \boldsymbol{B}(\boldsymbol{r}) &= \boldsymbol{B}_\infty(\boldsymbol{r}) - \boldsymbol{B}_{\rm vol}, \\ \boldsymbol{B}_{\rm vol} &= \frac{\mu_0}{4\pi}\sum_{l=1}^{m}(\sigma_l^- - \sigma_l^+)\int_{S_l}\Phi(\boldsymbol{r}')\boldsymbol{n}{\rm d}s'\times\frac{\boldsymbol{R}}{|\boldsymbol{R}|^3}, \\ \boldsymbol{B}_\infty(\boldsymbol{r}) &= \frac{\mu_0}{4\pi}\int_{V_{\rm H}}\boldsymbol{J}_{\rm P}(\boldsymbol{r}')\times\boldsymbol{R}/|\boldsymbol{R}|^3{\rm d}V'_{\rm H}, \qquad (5) \end{aligned}$$

where $\Phi_\infty(\boldsymbol{r})$ and $\boldsymbol{B}_\infty$ are the potential and the magnetic field in an infinite homogeneous medium, generated by the primary current density $\boldsymbol{J}_{\rm P}$ in the cardiac region $V_{\rm H}$. The surface S_l $(l = 1, 2, \ldots, m)$ is the closed interface between different conductivity regions, which separates the homogenous media of isotropic conductivities σ_l^+ on the outside and σ_l^- on the inside. $\bar{\sigma}$ is the mean conductivity. In the cardiac electromagnetic field calculation, cardiac equivalent source models are often used to represent the cardiac electric activities and to calculate $\Phi_\infty(\boldsymbol{r})$ and $\boldsymbol{B}_\infty$. The dipole source model and the EDL source model are used in this study.

Based on the bidomain equations, the equivalent dipole source for isotropic myocardium $\boldsymbol{J}_{\rm P}$ can be calculated from transmembrane potential (TMP) Φ_m as[27]

$$\boldsymbol{J}_{\rm P} = -\sigma_{\rm i}\nabla\Phi_m\delta(\boldsymbol{r}'), \tag{6}$$

where $\sigma_{\rm i}$ is the macroscopic intracellular conductivity and $\delta(\boldsymbol{r}')$ is the Dirac delta function. The dipole is represented by six parameters: three for location $\boldsymbol{r}'$ in Cartesian coordinates and the other three for the moment as the gradient components of the transmembrane potentials in Cartesian coordinate system. The

lumped dipole source is the sum of many cellular unit dipoles. Substituting Eq. (6) into Eq. (4), the $\Phi_\infty(\boldsymbol{r})$ can be expressed as

$$\Phi_\infty(\boldsymbol{r}) = \frac{1}{4\pi\sigma_\mathrm{s}} \int_{V_\mathrm{H}} -\sigma_\mathrm{i} \nabla \Phi_m \cdot \nabla \frac{1}{\boldsymbol{R}} \mathrm{d}V'_\mathrm{H}. \quad (7)$$

If the anisotropy ratios of the inner domain and the outer domain in the bidomain model are equal, the dipole moment with the gradient of the TMP as Eq. (7) can be replaced by the TMP as the EDL source through the vector calculus[28]

$$\Phi_\infty(\boldsymbol{r}) = \frac{1}{4\pi\sigma_\mathrm{s}} \int_{S_\mathrm{H}} -\sigma_\mathrm{i} \Phi_m \nabla \frac{1}{\boldsymbol{R}} \cdot \boldsymbol{n} \mathrm{d}S'_\mathrm{H}. \quad (8)$$

Comparing Eq. (7) with Eq. (8) shows that the volume integral is transformed into a surface integral, and the gradient of the TMP is replaced by TMP, from dipole source to EDL source. The EDL source model is the distributed source model, which includes the endo-cardial surface and the epi-cardial surface of the ventricle. The strength of the EDL source is equivalently described by the TMP. For more details about the dipole and EDL source, please refer to the publication[23] and the references in it.

With a similar procedure, the $\boldsymbol{B}_\infty$ calculated from the dipole and EDL source can be expressed as

$$\boldsymbol{B}_\infty(\boldsymbol{r}) = \frac{\mu_0}{4\pi} \int_{V_\mathrm{H}} \sigma_\mathrm{i} \nabla \Phi_m \times \nabla \frac{1}{\boldsymbol{R}} \mathrm{d}V'_\mathrm{H}, \quad (9)$$

$$\boldsymbol{B}_\infty(\boldsymbol{r}) = \frac{\mu_0}{4\pi} \int_{S_\mathrm{H}} \sigma_\mathrm{i} \Phi_m \nabla \frac{1}{\boldsymbol{R}} \times \boldsymbol{n} \mathrm{d}S'_\mathrm{H}. \quad (10)$$

3. Simulation protocol

The MCG simulation study is implemented based on the virtual heart electric model (LFX), which was developed by our group.[29,30] The original anatomic model including the heart and volume conductor model was obtained from the computed tomography (CT) scans of a human. The constructed heart model consists of approximately 65000 myocardial units with a spatial resolution of 1.5 mm. The main electrical conduction system, consisting of an atria-ventricular node, a His bundle, left and right bundles and Purkinje fibres, is designed according to cardiac physiology. After setting action potential wave forms and excitation propagation velocities for different myocardial units, the electrical excitation simulation is realized and the activation time of each unit is obtained. In this study, only the ventricular part was used for the MCG simulation. Figure 1(a) displays the ventricle part with activation time information from 0 to 61ms. The locations of the single-dipole source (DIP_I) and 53-dipole source (DIP_II) are shown in Fig. 1(b), in which the DIP_I is indicated as a large sphere and the DIP_II are shown as the small spheres. The DIP_I is located in the centre of the ventricle 9.6 cm away from the MCG measurement plane. The DIP_II with 53 lumped dipoles are calculated based on the segmentations of the ventricle by summing the cellular dipoles in each region.[30] While for the EDL source, the whole closed ventricular surface including endo- and epi-cardial surfaces with 7082 nodes and 14160 triangular elements is taken in this study.

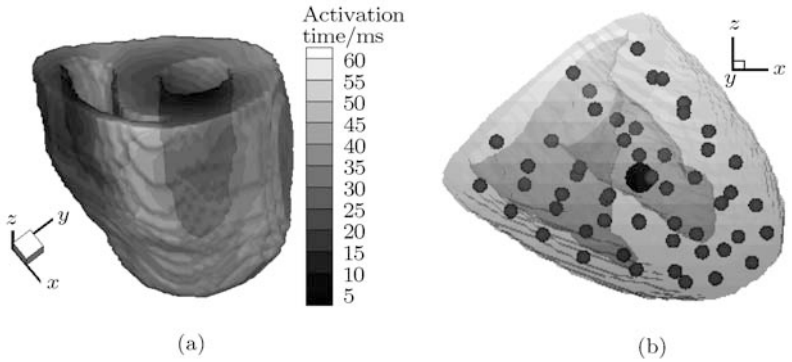


Fig. 1. Virtual heart model with ventricular part: (a) the activation time of the ventricular part, (b) the locations of dipole sources: 53 small spheres for DIP_II and one large sphere for DIP_I.

The mesh of torso volume conductor model is shown in Fig. 2, which includes the lung. The lung has 297 nodes and 586 elements, while the torso has 412 nodes and 820 elements. The conductivities of the lung and the torso are 0.04 and 0.2 siemens/m respectively. To simulate a realistic measurement situation, the MCG is calculated on the 130 points in an area of 25 cm×30 cm, 3 cm distance from the frontal chest as shown in Fig. 2. With regard to the Cartesian coordinate system, the measured MCG is the normal component as the one in the

$-y$ direction in this study, labeled as B_y, which is to be used in the following text. The infinite homogeneous magnetic field $\boldsymbol{B}_\infty$ is compared with the total field $\boldsymbol{B}$ to check the effect of the volume conductor model.

The differences between MCGs generated from different source models and volume conductor models are evaluated with a relative error (RE) and a correlation coefficient (CC).[22]

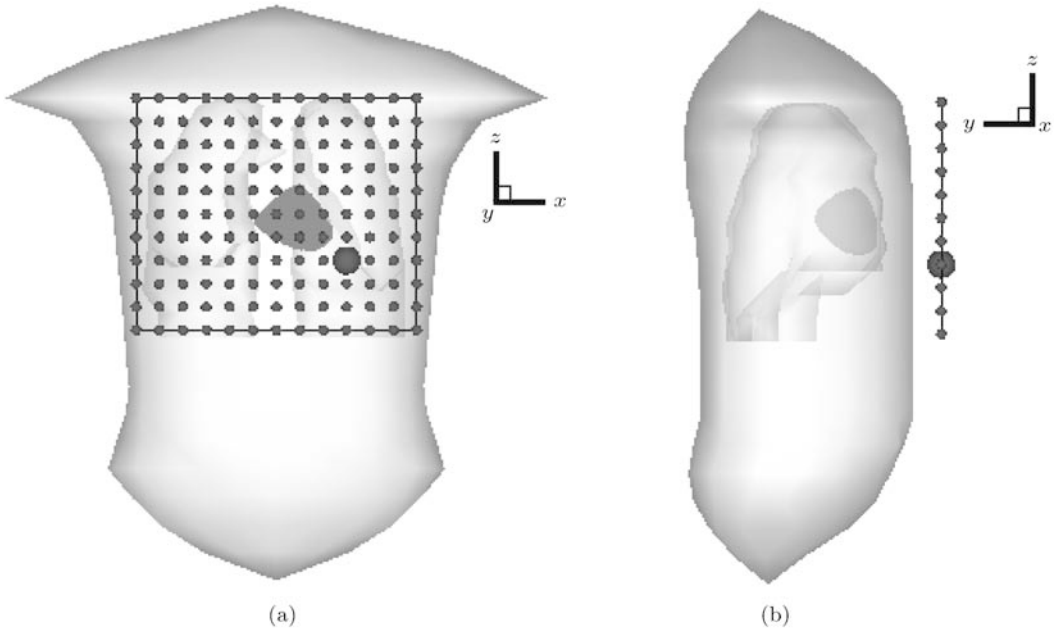


Fig. 2. Torso volume conductor model: (a) the anterior view and (b) the side view. The 130 small spheres are the locations of calculated MCG, while the one large sphere is used to show the MCG signal curve in Fig. 4(b).

4. Results

4.1. Cardiac equivalent source models

The MCG is first simulated based on the inhomogeneous volume conductor model from dipole and EDL sources. The body surface potential (BSP) is normalized into 1 mV, then the MCG is normalized as the same scale. Figure 3 shows the MCGs at Q, R, S and T wave instants: 3 ms, 30 ms, 51 ms and 246 ms, generated by sources: DIP_I (a), DIP_II (b) and EDL (c). The BSPs generated by the source DIP_II (d) are also displayed for comparison. It can be seen that the main distributive characteristics of the simulated MCG are similar to the measured ones, and the distributions of electric and magnetic fields are orthogonal to each other. The three source models can generate similar MCGs most of the time, however, the MCG from the DIP_I source is very different from those from the other two sources, e.g. the MCG at T wave time instant.

To quantitatively check the difference among the three cardiac source models for each time, we compare the MCGs generated by DIP_I and EDL sources with the one by DIP_II as the reference one. Figure 4 shows the CCs for DIP_I and EDL. We can see that the results of EDL are much closer to those of the DIP_II most of the time, while the ones of DIP_I are very different due to the lower resolution. However, the difference between the MCG generated by EDL from that by DIP_II becomes larger after the T wave time instant, and it reaches a maximal value at the 348 ms as shown in Fig. 4(c). Here, the large differences of the EDL source from the DIP_I and the DIP_II are due to the fact that the EDL is expressed only with the cells on the ventricular surface. At the end of the T wave, the ventricle has finished repolarization. Therefore, the cardiac information included in the EDL source is less than that included in the DIP_I and DIP_II sources. However, when we further check the MCG signal curves at the locations shown in Fig. 2 (see Fig. 4(b)) and the MCG distributions (see Fig. 4(c)) for minimal CC time instant (348 ms), we can see that at these time instants the MCG signals are very weak (< 0.001 pT) and can be approximated to zero with considering the SQUID precision of measurement. Besides, the MCG signals at the time instants after the T wave include less diagnostic information about cardiac diseases. In addition, the small CC for the EDL appears mainly after the T wave, therefore, the EDL is accurate and more suitable for MCG simulation compared to the DIP_I source.

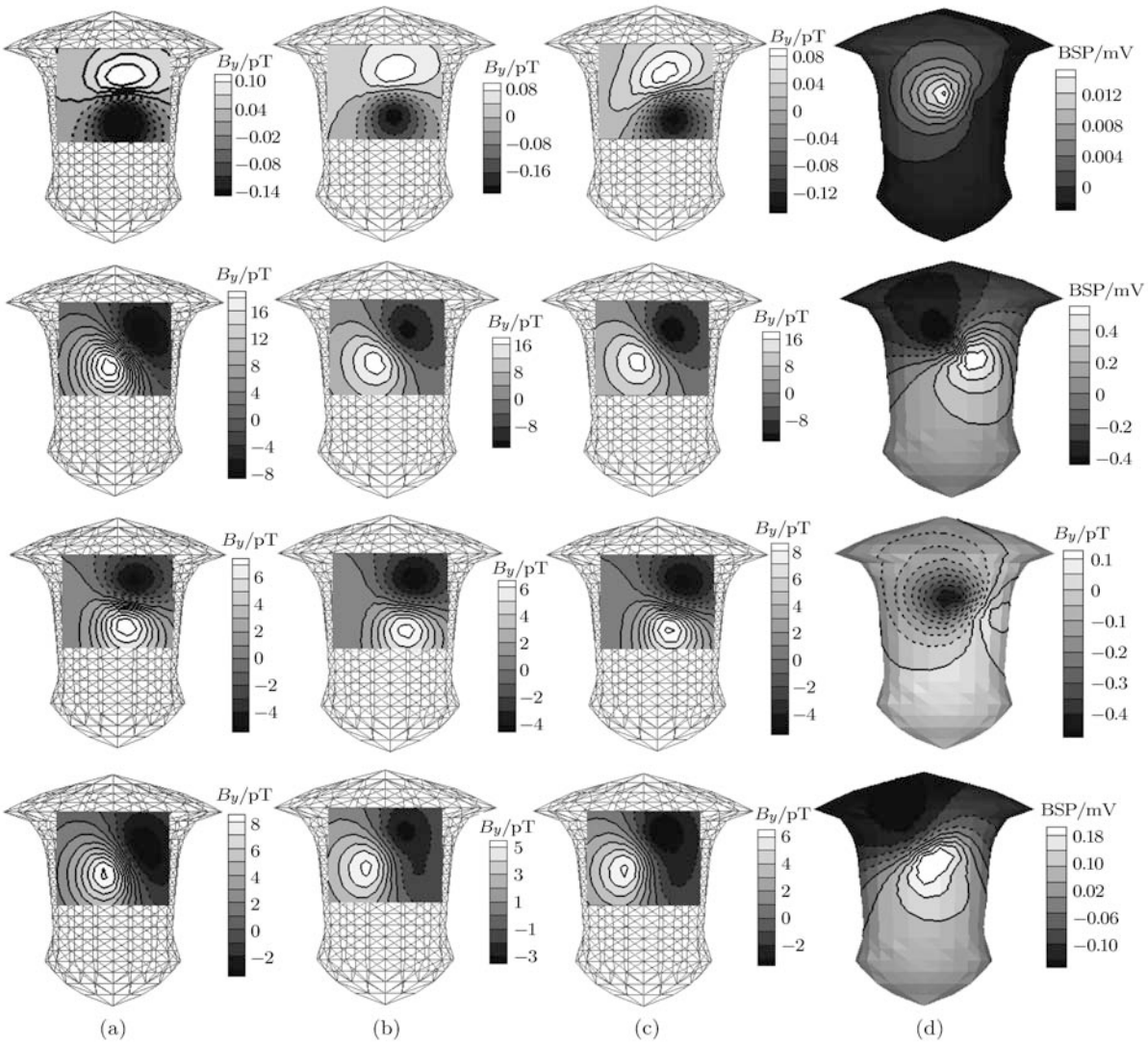
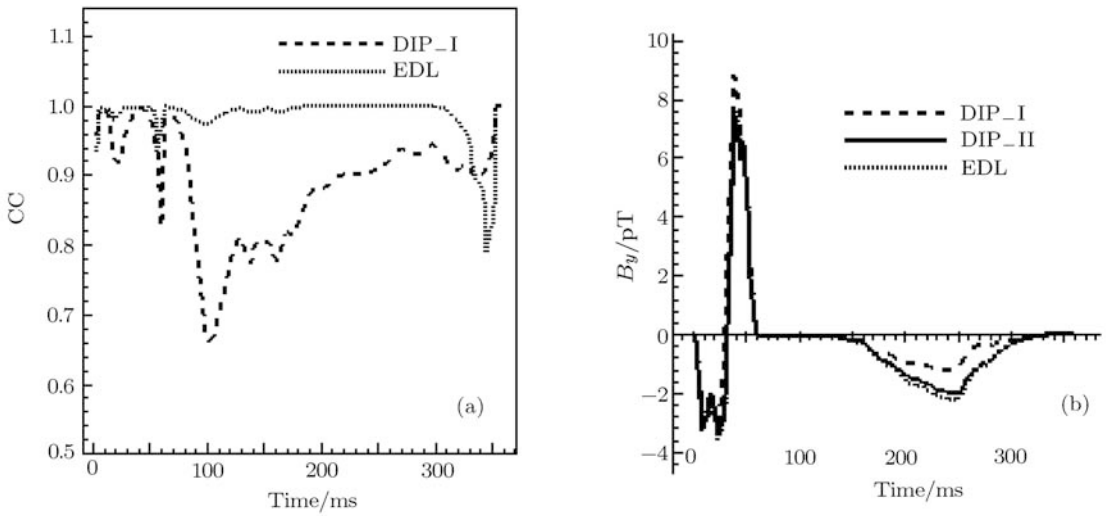


Fig. 3. The simulated MCG generated by sources: DIP_I (a), DIP_II (b), and EDL source (c), and the BSP generated by DIP_II (d). From top to bottom are the results for Q, R, S and T wave time instants.



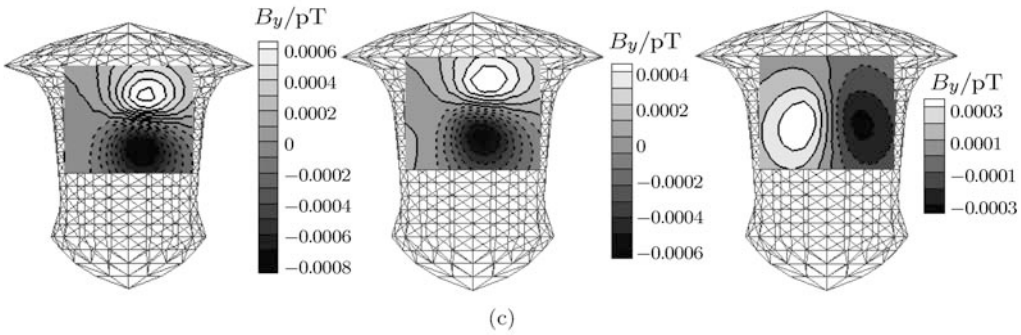


Fig. 4. (a) The MCG CCs calculated from DIP_I and EDL sources with the MCG of DIP_II source taken as the reference one, (b) the MCG signal curves at the locations shown in Fig. 2, and (c) MCG distributions at 348 ms with a minimal CC for EDL source. The dot line is for EDL source, the dash line for DIP_I, and the solid line for DIP_II in panels (a) and (b). The MCG distributions from left to right in panel (c) are generated by DIP_I, DIP_II and EDL sources, respectively.

4.2. Volume conductor model

The volume conductor model can affect the cardiac electromagnetic field as a secondary source. Its influence on the electric field is larger than that on the magnetic field, therefore, it was often left out in previous MCG studies and always acts as an infinite homogeneous medium.[20,22] In the present study, the contribution of the volume conductor model to the MCG is investigated in detail based on the virtual heart model. In fact, the magnetic field of the infinite homogeneous medium is $\boldsymbol{B}_\infty$. Figure 5 shows the CCs and the REs between $\boldsymbol{B}_\infty$ and $\boldsymbol{B}$ for DIP_I, DIP_II and EDL sources, with the $\boldsymbol{B}$ taken as a reference value. We can see that the volume conductor model has little effect on the MCG distribution (large CC), which is helpful for the inverse solution. The effect is smallest for the EDL source. The different volume conductor effects can be explained by the distance of the source point from the inhomogeneous lung region, and the distance is larger for dipole source than that for the EDL source. As an example, the distributions of infinite homogeneous magnetic field $\boldsymbol{B}_\infty$, volume conductor magnetic field $\boldsymbol{B}_{\rm vol}$ and their resultant field $\boldsymbol{B}$, i.e., $\boldsymbol{B}_\infty - \boldsymbol{B}_{\rm vol}$ in the measurement plane, calculated from three source models at the time with the smallest CC (24 ms), are shown in Fig. 6. Here, only the normal component of the magnetic field is shown in order to make it consistent with the MCG measurement.

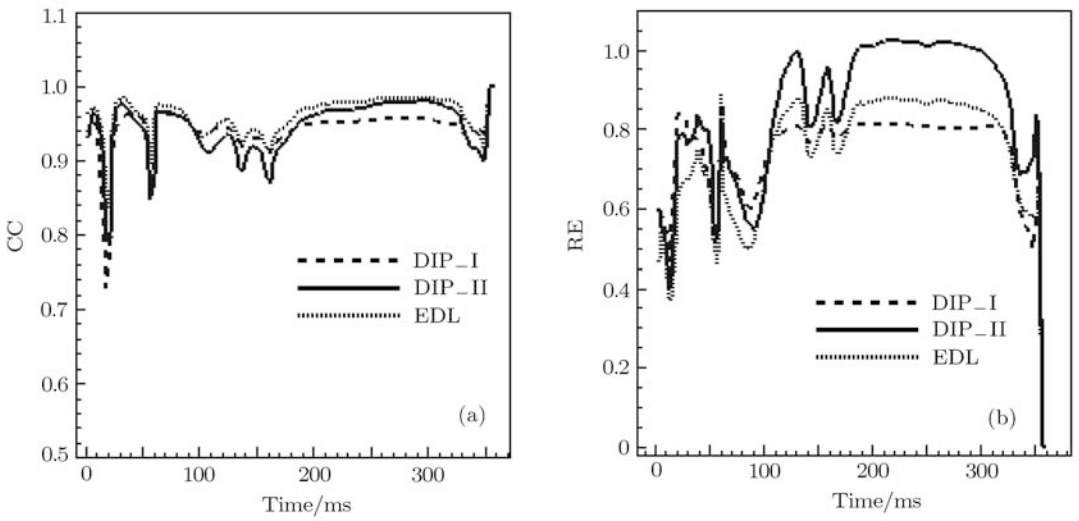


Fig. 5. Statistic results of CC (a) and RE (b) for the infinite homogeneous magnetic field $\boldsymbol{B}_\infty$, which are evaluated with the resultant magnetic field $\boldsymbol{B}$ as the reference one.

It can be seen that the magnitude of the $\boldsymbol{B}_\infty$ is larger than that of the $\boldsymbol{B}_{\rm vol}$, and the secondary magnetic field $\boldsymbol{B}_{\rm vol}$ weakens the primary field $\boldsymbol{B}_\infty$ as implied by the minus sign before $\boldsymbol{B}_{\rm vol}$ in Eq. (5). The $\boldsymbol{B}_\infty$ for DIP_I

source is symmetric, while the $\boldsymbol{B}_\infty$ fields for DIP_II and EDL sources are asymmetric, which is due to the more complicated distributions of these two source models. In addition, the distribution of the $\boldsymbol{B}_\infty$ is more regular than that of the $\boldsymbol{B}_{\rm vol}$: more extreme values exist in the $\boldsymbol{B}_{\rm vol}$, which is due to the geometrical complicacy of the volume conductor model. Considering the dependence of the performance of the volume conductor model on the source model, the volume conductor model should be considered in the cardiac magnetic field calculation to simulate a more accurate MCG.

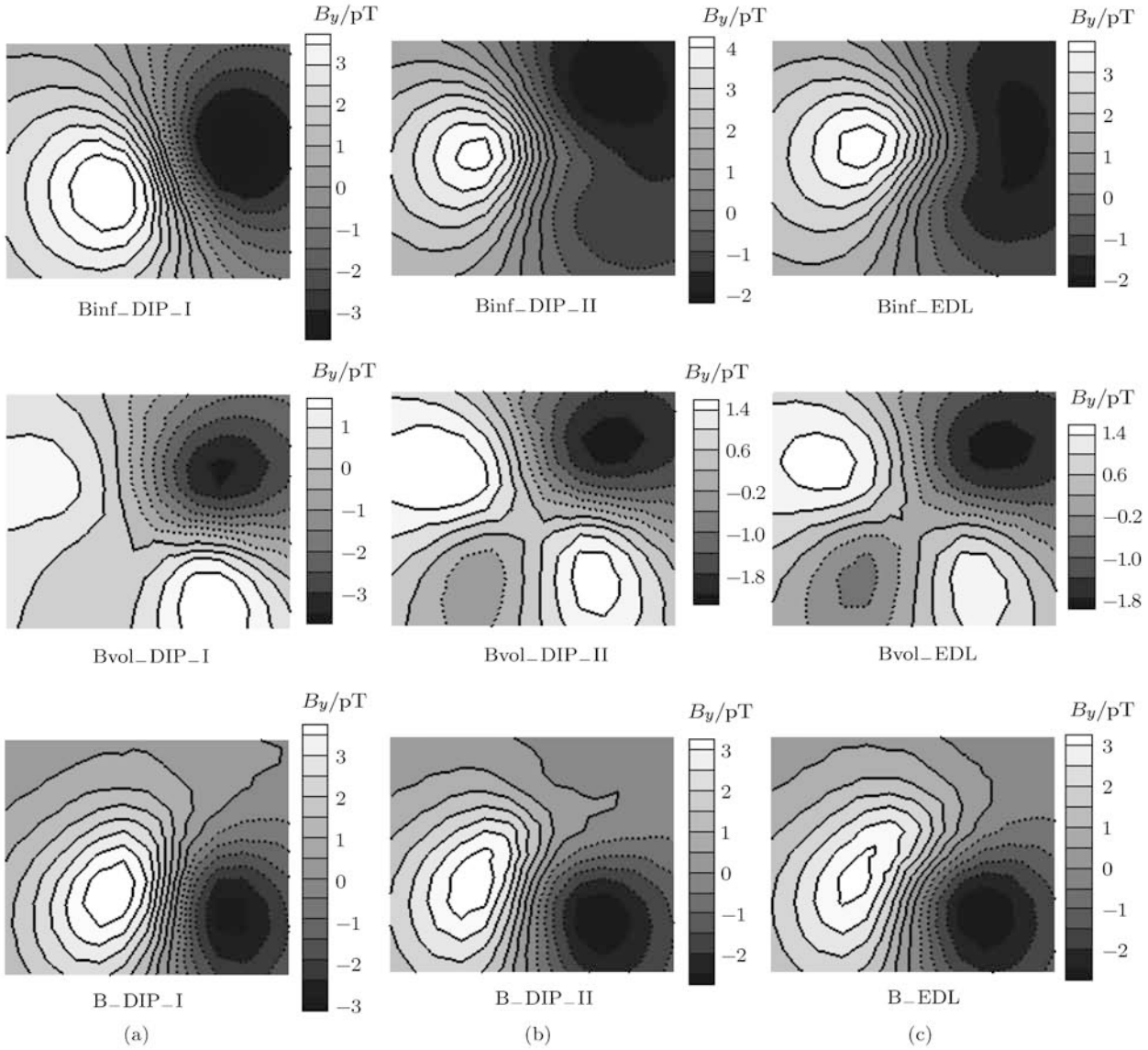


Fig. 6. Normal components of the three different magnetic field distributions in the measurement plane for the time instant with smallest CC (24 ms) from sources (a) DIP_I, (b) DIP_II and (c) EDL. Infinite inhomogeneous magnetic field $\boldsymbol{B}_\infty$, volume conductor magnetic field $\boldsymbol{B}_{\rm vol}$ and total field $\boldsymbol{B}$ as ($\boldsymbol{B}_\infty - \boldsymbol{B}_{\rm vol}$) are shown from top to bottom.

5. Conclusion

In this paper, the different contributions of the cardiac source models and the volume conductor model are systematically analysed and compared based on a MCG simulation with a virtual human heart model. In the study of cardiac source models, the results of a 53-dipole source are set to be a reference to investigate the single dipole source and the EDL source. The single dipole source is often used in MCG study, while the EDL is seldom concerned. The simulated results demonstrated that the MCG from DIP_I is much different from that from DIP_II, which means that the cardiac information is partly missed for the forward simulation of BSP or MCG from the DIP_I source. Figures 3 and 4 also demon-

strate that the DIP_I is less inaccurate at QRS time instants than at other time instants. However, the simple representation of the DIP_I source makes up for its deficiency in cardiac information, thereby making the DIP_I source commonly and successfully used in source location studies. The EDL source can generate a similar MCG to that from the DIP_II source.

The simulated results of the volume conductor model show that the effect is more important on the MCG magnitude than on the MCG spatial distribution. Therefore, it might be possible to just multiply the result with a factor to offset the inhomogeneous volume conductor effect. However, the factor value depends not only on the property of the volume conductor model but also on the source model used, due to the various contributions of the volume conductor to the MCG as shown in this study. Therefore, more detailed studies are needed to appropriately determine the factor value. The smallest effect of the EDL source on the volume conductor model also suggests the rationality and effectiveness of the EDL source, though it is seldom used in MCG compared with the dipole source. From a diagnostic viewpoint, the EDL is directly related to the electrophysiological characteristics of heart-like activation times, ectopic pacemakers, conduction blocks, etc., which can be easily and directly understood by clinicians. However, the dipole source is more complicated for clinicians to use and needs some physical knowledge relevant to certain cardiac diseases. Of course, the application of the EDL source needs more work on the heart anatomy information collected by imaging. With the advancement of imaging modalities such as high-field MRI and the image process techniques, obtaining information about heart anatomy will become much easier, which will further promote the application of the EDL source. However, the advantages of the EDL source make it valuable.

In all, in the presented study we suggested that the EDL source could be considered as an appropriate option for future MCG study and should receive more attention.

References

[1] Dos Santos R W, Kosch O, Steinhoff U, Bauer S, Trahms L and Koch H 2004 *J. Electrocardiol.* **37** 123

[2] Lim H K, Chung N, Ko Y G, Lee Y H and Park Y K 2009 *IEEE Trans. Magn.* **45** 2890

[3] Im B U, Kwon S S, Kim K, Lee Y H, Park Y K, Youn C H and Shim E B 2008 *Prog. Biophys. Mol. Biol.* **96** 339

[4] Smith F E,Langley P, van Leeuwen P, Hailer B, Trahms L, Steinhoff U, Bourke J P and Murray A 2007 *Anadolu Kardiyoloji. Derg.* **7** 20

[5] Yamada S and Yamaguchi I 2005 *Intern. Med.* **44** 1

[6] Fenici R, Brisinda D and Meloni A M 2005 *Expert Rev. Mol. Diagn.* **5** 291

[7] Jurkko R, Mantynen V, Tapanainen J M, Montonen J, Vaananen H, Parikka H and Toivonen L 2009 *Europace* **11** 169

[8] Wang C N, Li W Q, Zhang J and Fang P H 2006 *Chin. J. Med.* **41** 9 (in Chinese)

[9] Koch H 2001 *IEEE Trans. Appl. Supercond.* **11** 49

[10] Liu X Y, Xie F X, Meng S C, Ma P, Yang T, Nie R J, Wang S Z, Wang F R and Dai Y D 2003 *Acta Phys. Sin.* **52** 2580 (in Chinese)

[11] Zhao L, Chen G H, Zhang L H, Huang X G, Zhai G J, Li J W, Tang Y L and Feng J 2004 *Acta Phys. Sin.* **53** 4420 (in Chinese)

[12] Liu X Y, Xie B Q, Dai Y D, Wang F R, Li Z Z, Ma P, Xie F X, Yang T and Nie R J 2005 *Acta Phys. Sin.* **54** 1937 (in Chinese)

[13] Zhang S L, Wang Y L, Wang H W, Jiang S Q and Xie X M 2009 *Phy. Med. Biol.* **54** 4793

[14] Ogata K, Kandori A, Miyashita T, Tsukada K, Nakatani S, Shimizu W, Kanzaki H, Miyatake K, Yamada S, Watanabe S and Yamaguchi I 2006 *Int. J. Cardiovasc. Imag.* **22** 581

[15] Ramon C, Czapski P, Haueisen J, Huntsman L L, Nowak H, Bardy G H, Leder U, Kim Y and Nelson J A 1998 *IEEE Trans. Biomed. Eng.* **45** 1323

[16] Geselowitz D B 1980 *IEEE Trans. Magn.* **16** 812

[17] Czapski P, Ramon C, Huntsman L L, Bardy G H and Kim Y 1996 *Phys. Med. Biol.* **41** 1247

[18] Wang Q, Hua N, Lu H, Ma P, Tang F K and Tang X Z 2010 *Chin. Phys.* B **19** 080601

[19] Haueisen J, Schreiber J, Brauer H and Knosche T R 2002 *IEEE Trans. Magn.* **38** 1045

[20] Wang Q, Ma P, Hua N, Lu H, Tang X Z and Tang F K 2010 *Acta Phys. Sin.* **59** 2882 (in Chinese)

[21] De Melis M, Tanaka K and Uchikawa Y 2010 *IEEE Trans. Magn.* **46** 1203

[22] Wang Q, Ma P, Lu H, Tang X Z, Hua N and Tang F K 2009 *Chin. Phys.* B **18** 5566

[23] van Oosterom A 2003 *Int. J. Bioelectromagnetism* **5** 211

[24] Zhang L, Jiang S Q, Wang L, Luo M and Wang L M 2005 *Modern Scientific Instruments* **4** 31 (in Chinese)

[25] van Oosterom A, Oostendorp T F, Huiskamp G J and Terbrake H J M 1990 *Circ. Res.* **67** 1503

[26] Shou G F, Xia L, Jiang M F, Wei Q, Liu F and Crozier S 2009 *IEEE Trans. Biomed. Eng.* **56** 1454

[27] Gulrajani R M 1988 *Crc. Critical. Rev. Biomed. Eng.* **16** 1

[28] Yamashita Y and Geselowitz D B 1985 *IEEE Trans. Biomed. Eng.* **32** 964

[29] Xia L, Huo M, Wei Q, Liu F and Crozier S 2006 *Methods Inf. Med.* **45** 564

[30] Lu W X and Xia L 1996 *IEEE Trans. Biomed. Eng.* **43** 211